Improvement in motion correction technique for microPET brain imaging

Lin Zhou, Matthew Bickell, Andre Kyme, Roger Fulton and Johan Nuyts

***Abstract*— Motion correction (MC) in microPET brain imaging of awake small animals is attracting more interest in preclinical studies to avoid the confounding effects of anesthesia. One of the motion correction methods is to use a stereo optical camera to track the head motion of the animal, which is assumed to be represented by the motion of a tracking marker attached to its forehead. In the presented study, we explored several ways to improve the experimental setup as well as the reconstruction procedures of this method. These approaches include camera distance optimization, improved temporal synchronization of list mode events with motion tracker samples, post-acquisition pose interpolation, and list-mode reconstruction with appropriately selected subsets. These methods were first verified by reconstructing a resolution phantom that underwent continuous motion at different camera distances, and were then applied to a microPET brain scan of an awake rat. The results show that applying the proposed methods leads to a robust experimental setup and motion-corrected reconstructions with improved spatial resolution.**

I. Introduction

Motion correction (MC) for microPET brain imaging of awake small animals becomes more and more popular in preclinical studies. The main advantage of scanning awake animals is to avoid the confounding effects of anaesthesia. One of the motion correction methods is to use a stereo optical camera to track the head motion of the animal, which is assumed to be represented by the motion of a tracking marker attached to its forehead. Such a method was originally developed and validated by the University of Sydney [1], and was later implemented in the research lab of KU Leuven. In the presented study, we explored several ways to improve the experimental setup as well as the reconstruction procedures of this method. These approaches include camera distance optimization, improved temporal synchronization of list mode events with motion tracker samples, post-acquisition pose interpolation, and list-mode reconstruction with appropriately selected subsets. The proposed methods were first verified by reconstruction a moving resolution phantom, and were then applied in a real rat experiment.

II. Methods

A. Camera distance optimisation

The stereo optical camera used for motion tracking is the MicronTracker Sx60 (MT, Claron Technology Inc., Toronto, Canada) which has a fixed focal distance of 70 cm. To make the rat comfortable during the microPET acquisition, the marker to be attached to its forehead should be as small as possible, limiting the length of the marker to less than 10 mm. Based on our experience, the poses (position and orientation) of such a small marker can sometimes not be detected at the focal distance, and the detected poses are subject to a significant amount of jitter. To improve the sensitivity and the accuracy of small marker detection, we made the hypothesis that, when operating at distances closer than the focal range, the improvement in marker detection due to the subsequent magnification effect may outweigh the out-of-focus blurring. If this was the case, detecting a small marker may benefit from putting the MT much closer to the microPET scanner.

We aimed to verify this hypothesis and to find a MT distance (range) that is optimal for small marker detection. To this end, an industrial robotic arm (Epson C3-A601S 6-axis, SEIKO Corp., Japan) with repeatability of ± 20 μm was used to move the small marker through several controlled motion sequences and to provide the ground truth of the marker motion. The robot system and the MT system were cross-calibrated [1]. For the same motion sequences, the pose of the small marker was measured by the MicronTracker at different MT distances. The measured motion of the small marker was then compared to the applied motion, as a function of the MT distance.

We use T_i^S and T_i^R to indicate the 4×4 matrices of the i-th small marker pose and the i-th robot pose in the MT coordinate system, respectively. Each matrix involves 6 degrees of freedom (3 translations and 3 rotation angles) since we only consider rigid motion. The corresponding incremental motions are denoted by ΔT_i^S and ΔT_i^R, calculated as

$$\Delta T_i^S = T_i^S (T_{i-1}^S)^{-1} \tag{1}$$

$$\Delta T_i^R = T_i^R (T_{i-1}^R)^{-1} \tag{2}$$

For evaluation, a spherical grid of points centered on a virtual microPET field of view (FOV) was simulated. We set the radius of the sphere to 10 mm and assume that it is similar to the size of the rat brain. Using X_p to represent the coordinates of the p-th point on the grid in the MT coordinates, and applying the incremental motions to this point results in the transformed points $X_{p,i}^S$ and $X_{p,i}^R$:

$$X_{p,i}^S = \Delta T_i^S X_p \tag{3}$$

$$X_{p,i}^R = \Delta T_i^R X_p \tag{4}$$

We can then calculate the distances between these transformed points:

$$D_{p,i}^{S-R} = \| X_{p,i}^S - X_{p,i}^R \| \tag{5}$$

The closeness of the transformed points represents the similarity of the detected poses. Using the robot pose as the gold standard, a smaller $D_{p,i}^{S-R}$ indicates a better accuracy of the small marker detection.

To evaluate the overall performance of MT detection at a

L. Zhou, M. Bickell and J. Nuyts are with the Medical Imaging Research Center, KU Leuven, Belgium. A. Kyme and R. Fulton are with the Brain and Mind Research Institute, the University of Sydney, Australia.

This work is supported by IMIR project of KU Leuven.

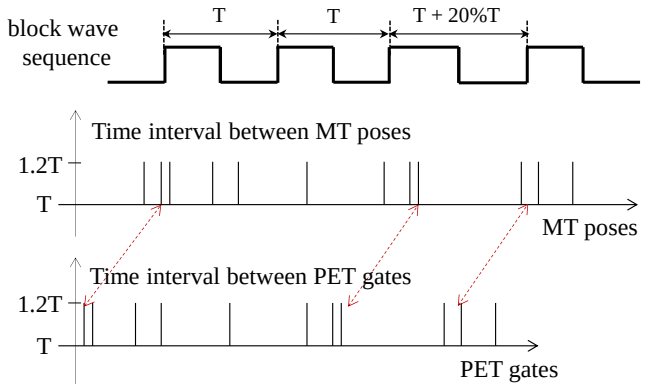

Fig. 1. Synchronization using new signal generator. The length of each block signal has a probability of 1/32 to be increased by 20%. The same pattern will propagate to the time intervals between both MT poses and PET gates, which makes synchronization much more robust.

certain distance, we use the following measurements:

$$\bar{D}^{S-R} = \frac{1}{N_i}\sum_{i=1}^{N_i} \bar{D}_i^{S-R} \tag{6}$$

$$\bar{\sigma}^{S-R} = \frac{1}{N_i}\sum_{i=1}^{N_i} \bar{\sigma}_i^{S-R} \tag{7}$$

where N_i is the total number of incremental poses acquired at that MT distance, and $\bar{D}_i^{S-R}$ and $\bar{\sigma}_i^{S-R}$ are the mean and the standard deviation of $D_{p,i}^{S-R}$ over all the points on the grid.

B. Synchronization using a novel signal generator

A standard approach to achieve temporal synchronization between the MT motion data and the microPET list-mode data, a regular block wave from a signal generator is used as externally trigger the MT. At each high-to-low transition of the trigger signal, the MT records a pose which is stored on a PC, and it also sends a strobe output to the microPET gate input, ensuring that a gate entry is inserted in the list-mode data file [1]. Synchronization is then achieved by aligning the first (or last) pose with the first (or last) gate. The reliability of this alignment is difficult to determine since poses or gates may have been missed, and only the quality of the reconstruction can suggest that the synchronization may have been suboptimal.

In order to improve upon this, we developed a signal generator that produces a regular block wave pattern, but every block wave has a probability of 1/32 of having its length increased by a predetermined factor (20%). This is achieved with a 16 bit pseudo-random generator, and introduces an irregular and unique pattern to the periods between the MT poses and microPET gates. This pattern has a period of $2^{16}-1$ triggers, or about 35 min at a triggering frequency of 30 Hz. The presence of the pattern provides a means for a robust synchronization.

C. Optimized delay time for pose-to-gate correlation

Between the recording of the poses and the insertion of the gate tags there is a delay. This delay depends on various factors such as the sampling frequency, the exposure time of the camera, the width of the strobe signal sent to the microPET, and the communication time between the MT and the microPET. Some of these factors are accurately known but some are difficult to predict. This delay time should be taken into consideration correctly before motion correction.

Fig. 2. Selecting events for different subsets: suppose we have 9 events in total, which are divided into 3 subsets (a) in the temporal order, (b) with the proposed method.

We are developing a data driven approach to estimate this delay time for the pose-to-gate correlation. The idea is as follows: 1) Align MT poses to microPET gates assuming that the delay time is t (in milliseconds); 2) motion correct all LORs; 3) back-project the MC-LORs, and calculate the maximal value in the back-projection; 4) repeat steps 2 and 3 with different t values; 5) the t corresponding to the overall maximal value is the best delay time.

D. Pose interpolation

Poses are recorded by the motion tracking device at the frequency of the trigger signal, typically on the order of 30 Hz. Therefore, for rapid motion the subject can move up to a few millimeters between poses. Performing a linear interpolation between poses will reduce the blur introduced by this inter-pose motion. To reduce the affect of jitter, the measured poses were smoothed before interpolation [3]. Without pose interpolation, each recorded pose is treated as the average pose over a time interval about that pose. However, when interpolating between the poses the recorded pose should then be treated as the pose at the start of that time interval. Thus the pose-to-gate delay must increase by half a pulse width when performing pose interpolation.

E. Subset selection

In our study, list-mode reconstruction is applied to incorporate all detected events [4]. Before reconstruction, the orientation of each line of response is corrected according to the measured motion. Subsets are used to speed up the convergence of the reconstruction. In order to make the events in each subset more representative for the entire dataset in the presence of motion, we propose that the events in each subset should be selected along the whole list-mode stream (Fig. 2(b)) rather than in a temporal order (Fig. 2(a)). During the reconstruction, the time-averaged sensitivity matrix was calculated in the image domain, as proposed in [4]. With this subset selection procedure, the same sensitivity image can be used for all subsets.

III. Experiment

A. Camera distance optimization

For distance optimization, three types of motion (complex motion, rat-like motion and step motion) were executed by the Epson robot. The distance range was from 285 mm to 575 mm. The data were acquired on two separate days, for large distances (479-575 mm) and small distances (285-460 mm), respectively. The MT data and the robot data were post-processed and compared as described in section II-A.

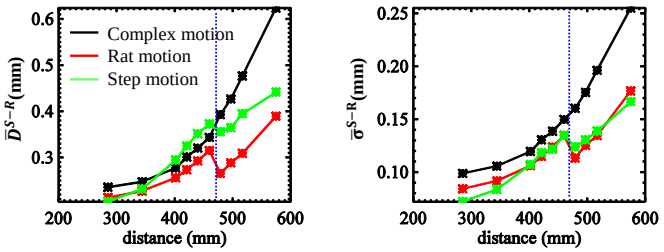

Fig. 3. The averaged distances ($\bar{D}^{S-R}$, left) and the averaged standard deviations of the distances ($\bar{\sigma}^{S-R}$, right) between the transformed points. The dashed line distinguishes the data acquired on two separate days.

B. MicroPET scans

We verified the proposed methods with microPET experiments. First, a phantom scan was performed to estimate the influence of different motion correction settings, and then the best settings were used in a rat experiment. The novel signal generator was applied throughout the experiment.

1) Phantom scan: A resolution phantom consisting of hot rods with various diameters (1.5 mm - 3.0 mm) filled with 0.9 mCi of ^{18}F-FDG was scanned and the phantom was moved by a toy robotic arm. The motion tracking sampling frequency was 29 Hz. The motion data and the microPET list-mode data were acquired with three MT distances (44 cm - 56 cm - 68 cm). For each MT distance, we applied different motion correction settings: with/without pose interpolation and with/without optimized delay time. The lines of response were re-orientated accordingly.

After data acquisition, the motion-corrected LORs were reconstructed using the proposed list-mode reconstruction, with 5 iterations and 10 subsets. The transaxial pixel size was 0.316 mm and the plane separation was 0.796 mm. A 3D Gaussian kernel with full width at half maximum (FWHM) of 1.3 mm was applied to model the resolution in the image domain. No attenuation or scatter correction was applied.

2) Rat scan: After the phantom scan, we applied the best settings (distance, delay time, pose interpolation) to a real rat scan. Prior to the scan we trained the rat for 4 days. During the training, the rat was placed in a transparent plastic tube in the microPET FOV, with the small marker attached to its forehead facing the MT. The aim of the training was to familiarize the rat with the motion-tracking environment. On the day of the scan the rat was injected with 470 μCi of ^{18}F-FDG. The first scan was done when it was fully awake. The scan was done 60 minutes post injection with 15 min duration. For comparison, we performed a second scan with the rat anesthetized using isoflurane. This scan was done 85 min post injection with duration of 20 min. The reconstruction parameters were the same as the phantom scan.

IV. Results

A. Camera distance optimization

The plot of the errors ($\bar{D}^{S-R}$, $\bar{\sigma}^{S-R}$) as a function of the MT distance is shown in Fig. 3. The results show that better detection accuracy can be achieved with a closer MT distance. However, one should consider the balance between the MT distance and the MT field of view, i.e., if the MT is too close to the microPET it cannot see the reference marker attached to the gantry of the microPET. Taking this into consideration, we chose 400-450 mm to be the optimized MT distance range and used it in the phantom and the rat experiments.

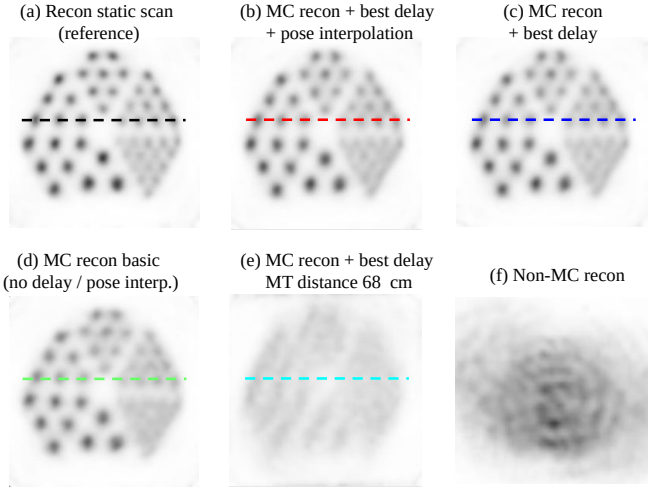

Fig. 4. Phantom reconstructions with different settings. All reconstructions are from data collected with the MT at a distance of 44 cm, except for the middle image in the lower row.

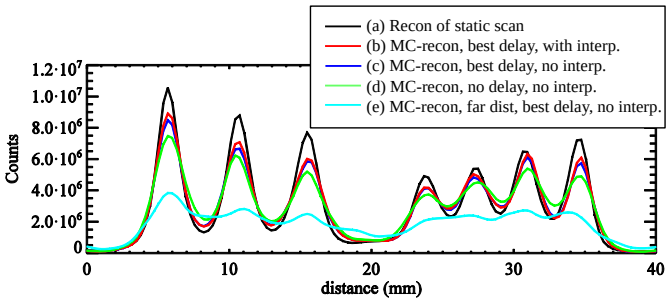

Fig. 5. Profiles through the reconstructions (a)-(e) in Fig. 4.

B. MicroPET scans

1) Phantom scan: The phantom reconstructions are shown in Fig. 4. Using the basic MC method (no pose interpolation, no optimized delay time) the reconstruction suffers from some resolution loss (Fig. 4(d)). Applying the optimized delay greatly improves the resolution in the MC reconstruction (Fig. 4(c)), leading to a MC reconstruction almost as good as the static scan (Fig. 4(a)). Pose interpolation produces slightly higher contrast in the hot rods (Fig. 4(b)). When the phantom was placed near the focal distance, the poses of the small marker were not as accurate as those at the optimized distance, resulting in a very blurred motion corrected reconstruction (Fig. 4(e)). Fig. 4(f) is the reconstruction without any motion correction. The profiles of the reconstructions through the dashed line are shown in Fig. 5.

2) Rat scan: The reconstructions of the rat are shown in Fig. 6. The resolution and contrast improved considerably after motion correction, showing good agreement with the reconstruction of the anesthetized rat.

V. Conclusion

We have presented several approaches to improve the experimental settings and the post-processing procedure of a motion correction technique used for microPET brain imaging. Applying these proposed methods leads to a robust experimental setup and well motion-corrected reconstructions. In the future, more work will be done to further eliminate the remaining resolution loss in the motion corrected reconstructions.

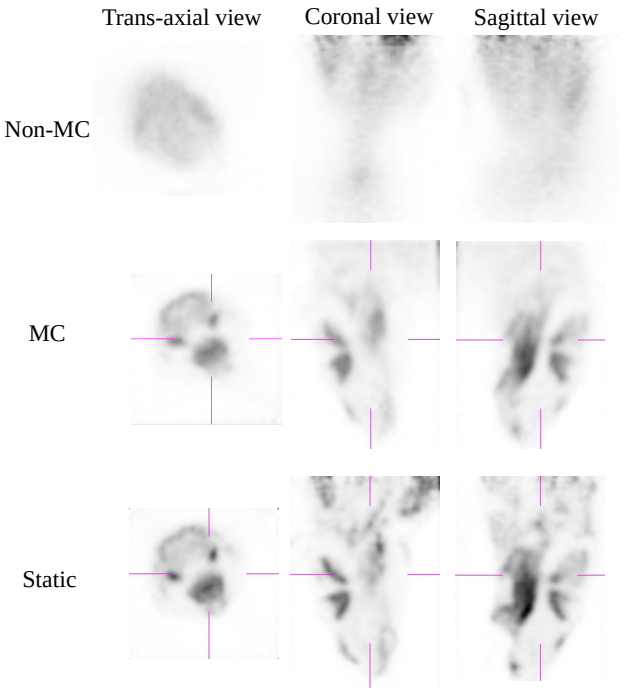

Fig. 6. Top row: reconstruction of awake rat without motion correction. Middle row: reconstruction of awake rat with motion correction. Bottom row: reconstruction of anaesthetized rat.

REFERENCES

[1] A. Z. Kyme, et al, "Optimised motion tracking for positron emission tomography studies of brain function in awake rats", *PLoS ONE*, 6(7), e21727, 2011.

[2] A. Z. Kyme, et al, "The effect of time domain pose filtering on accuracy of small marker based motion correction in awake animal PET", *IEEE NSS-MIC*, 2290-2294, 2011.

[3] A. Rahmin, et al, "Motion compensation in histogram-mode and list-mode EM reconstructions- beyond the event-driven approach", *IEEE Trans. Nucl. Sci.*, 51(5), pp. 2588-2596, 2004.